

Stability Analysis of the EFIE-IBC Formulation and Regularization via Spatial Filtering

Original

Stability Analysis of the EFIE-IBC Formulation and Regularization via Spatial Filtering / Bruliard, Margaux; Zucchi, Marcello; Vecchi, Giuseppe. - In: IEEE OPEN JOURNAL OF ANTENNAS AND PROPAGATION. - ISSN 2637-6431. - 6:2(2025), pp. 578-593. [10.1109/OJAP.2025.3538797]

Availability:

This version is available at: 11583/2997161 since: 2025-04-28T10:55:40Z

Publisher:

IEEE

Published

DOI:10.1109/OJAP.2025.3538797

Terms of use:

This article is made available under terms and conditions as specified in the corresponding bibliographic description in the repository

Publisher copyright

(Article begins on next page)

Received 14 November, 2024; revised 13 January, 2025; accepted 31 January, 2025; Date of publication XX Month, XXXX; date of current version 2 February, 2025.

Digital Object Identifier 10.1109/OJAP.2020.1234567

Stability Analysis of the EFIE-IBC Formulation and Regularization via Spatial Filtering

Margaux Bruliard¹ (Graduate Student Member, IEEE), Marcello Zucchi¹ (Member, IEEE), Giuseppe Vecchi¹ (Fellow, IEEE)

¹Department of Electronics and Telecommunications, Politecnico di Torino, 10129 Turin, Italy

CORRESPONDING AUTHOR: Margaux Bruliard (e-mail: margaux.bruliard@polito.it).

This work was supported by the European Union's Horizon 2020 research and innovation programme under the Marie Skłodowska-Curie grant agreement No 955476.

ABSTRACT The Impedance Boundary Condition (IBC) is a homogenization approximation of great importance, especially in the design of metasurfaces. However, the standard Electric-Field Integral-Equation formulation of the IBC boundary-value problem (EFIE-IBC) has been shown to lead to numerical instabilities for some impedance ranges of practical interest, in particular inductive reactances. This contribution shows that the numerical instabilities are due to an *intrinsic* ill-conditioning of the EFIE-IBC operator for the concerned surface impedance values, that can degenerate into an *ill-posedness* that does not allow for definite solution. Hence, the stable discretization of the EFIE-IBC operator requires a *regularization*. The analysis leads to a proposed regularization by systematically limiting the wavenumber spectrum of the basis functions, which amounts to a spatial filtering. This is implemented using entire-domain basis functions. Given the possible ill-posedness, we devise two “ground truth” test examples starting from a physical metasurface, then approximated via IBC. Comparison to ground truth results shows that the standard EFIE-IBC may lead to significant errors, and that these may be challenging to detect. Conversely, the regularized system yields stable results that well match the ground truth of the physical structure of which the IBC is an approximation.

INDEX TERMS Impedance Boundary Conditions (IBC), Electric Field Integral Equation (EFIE), Metasurfaces, Spectral basis functions (SBF), Method of Moments (MoM)

I. INTRODUCTION

A. OVERVIEW

The Impedance Boundary Condition (IBC) is a homogenization approximation for textured structures composed of “cells” that are sub-wavelength along two spatial directions, with the third usually not larger than one quarter wavelength. Loosely speaking, it consists of accounting for the “micro” scale details in terms of a relationship between tangential magnetic and electric fields. The most recent interest for IBC is in the analysis and design of metasurfaces; a metasurface is an electrically thin (i.e., not thicker than a quarter wavelength) and dense two-dimensional collection of structural elements called “unit cells”, also called (especially earlier on) “meta-atoms” [1]. Metasurfaces have been shown to effectively allow unprecedented field manipulations, like

flat broadside antennas, lenses, and more recently, Reflective/Reconfigurable Intelligent Surfaces (RIS) [2]–[4].

Historically, IBC has been used for decades [e.g., 5] in the analysis of composites and/or absorbing materials (like in RCS reduction), and in metal corrugations [e.g., 6]—most notably for horn antennas [7] and bull’s eye antennas [8].

Most often, in these applications, the IBC was one-sided, or “opaque”, i.e., defined on one half-space (for the simplest case of a planar surface) and meant to represent the entire structure below it. This was also the way the first seminal works on metasurface antennas [9], [10] used the IBC in *analytical* considerations. In this type of antenna, a guided wave leaks power to radiation due to impedance modulation; the need to have a guided, TM-type surface wave implies that the surface impedance has to be inductive.

As for the numerical simulation of IBC, we will concentrate here on the Integral-Equation Method of Moments (IE-MoM) approach. For planar surfaces, the IBC is not too different from the equation for a PEC and essentially amounts to substituting zero impedance of the PEC with a non-zero appropriate value (see Sec. II.A); this formulation is called Electric-Field Integral Equation with IBC (EFIE-IBC).

Hence, the use of IBC in a code designed for PEC scatterers appears to be a simple addition. However, [11] reported that application of MoM to *inductive* one-sided IBC metasurfaces leads to unstable and wrong solutions. That occurrence had apparently never been reported before, perhaps because most applications were for lossy structures or for capacitive reactances. The remedy to the problem for those structures was to model only the thin metasurface layer as an IBC sheet and include the rest (a grounded dielectric slab) in the background – which entails a more complex Green’s function. That is, instead of an opaque (one-sided) use of the IBC, one should use a transparent (two-sided or “sheet”) IBC. The workaround is based on the fact that the two-sided IBC (of the sheet) turns out to be capacitive, for which the equation is stable. On the other hand, even using a dielectric background, an inductive, two-sided IBC sheet was still reported to be problematic.

Before [11], a similar problem was addressed in [12], which dealt with closed objects by using a PMCHWT-based formulation [13]; seen in comparison with [11], it appears that the key difference is the presence of the Magnetic-Field Integral Operator (MFIO) that is absent in the EFIE-IBC. As such, it appears that when one considers a finite-thickness slab, but for a typical small thickness, the advantage of that approach vanishes.

B. PURPOSE AND MOTIVATIONS

The purpose of this paper is to analyze the reason for the instability of the EFIE-IBC formulation for the inductive range of reactance values and provide a solution to that problem. The motivation for this study is two-fold.

- 1) For the transparent setting, there are applications for which limiting the surface reactance to capacitive-only values restricts the range of achievable performances or bars some. An example of this are metasurfaces achieving anomalous reflection [14], in the context of RIS and smart propagation environment [3]. Likewise, low-reflection multi-layer metalenses would profit from alternating capacitive-inductive layers. More generally, increasing the degrees of freedom of the surface impedance allows reducing the constraints on the design of metasurfaces, enlarging their capabilities and making their design more robust.
- 2) There are several practical applications that call for a thick structuring that requires using an opaque IBC to (approximately) represent the unit cells lying below the reference surface. Examples of this are the metal

pillars of “bed-of-nails” structures used in the sub-THz range [15], or high-impedance surfaces [16], [17].

C. INNOVATION

To the best of the authors’ knowledge, this is the first comprehensive analysis of the ill-conditioning of the EFIE-IBC for certain ranges of surface reactance values. Likewise, the presented analysis suggests a method to overcome such shortcoming. A very preliminary summary of a part of this work was presented in the conference paper [18].

D. TERMINOLOGY

We conclude with a note on the employed terminology. In the theoretical analysis, we will need the eigenvalue spectrum of the key integral operator. We will also need to consider the two-dimensional Fourier Transform (FT) of the fields and of the eigenfunctions of the above-mentioned operator; such a FT is also referred to as spectrum in the literature. To avoid confusion about the meaning of the word “spectrum”, we will use the following terminology: the Fourier transform of spatial fields will be called *wavenumber spectrum*, while the spectrum of the operator will be referred to as *eigenvalue spectrum*, sometimes shortened to *eigenspectrum*.

II. BACKGROUND

A. IMPEDANCE BOUNDARY CONDITION (IBC) APPROXIMATION

Consider a planar metasurface with sub-wavelength details, alternatively called “unit cells” or “meta-atoms”; they can be metal patterns (patches or holes in a metal sheet) or relieves like metal or dielectric pillars, like in “bed of nails” structures. The unit cell is sub-wavelength along the surface plane dimensions, while its height may in some instances be not thin; in these latter cases, it is typically of the order of a quarter-wavelength [15]. An example of a common thin-metal metasurface is shown in Fig. 1.

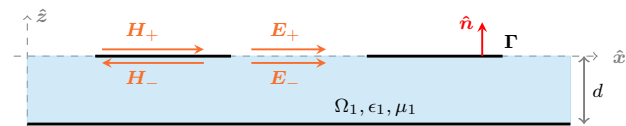


FIGURE 1. Cross-section of a typical metasurface consisting of a thin-metal texturing over a grounded dielectric substrate.

In the following, we will assume that the upper half space is free space, whereas all texturing and possibly dielectric and metal backing lie in the lower half space. The surface impedance boundary condition (IBC) is a homogenization approximation to simplify the analysis and—especially—the design of these structures. It represents the response of the sub-wavelength structure at a larger spatial scale via spatial averaging of both the tangential electric and magnetic fields. There are two main such IBC formulations [5], [11], graphically schematized in Fig. 2:

- 1) *Opaque* or one-sided IBC: in this case, the IBC represents the approximation of the entire lower half space, and the associated boundary value problem is the direct extension of a PEC plate in free space. Hence, as discussed below, the integral equation associated to this IBC employs the free space Green's function.
- 2) *Transparent*, or two-sided, or "sheet" IBC: in this case the IBC represents the approximation of only the textured surface. This can in principle entail a non-thin structure, with two separate sides linked by a transmission condition; however, in most cases, it is applied to a thin structure, i.e., representing a two-dimensional "sheet." The integral equation associated with this boundary problem includes all structures in the bottom half-space, and so does its Green's function. In this case, the situation where the structure consists of one or more dielectric layers can be accommodated with minor changes; the same holds as well for multiple impedance sheets.

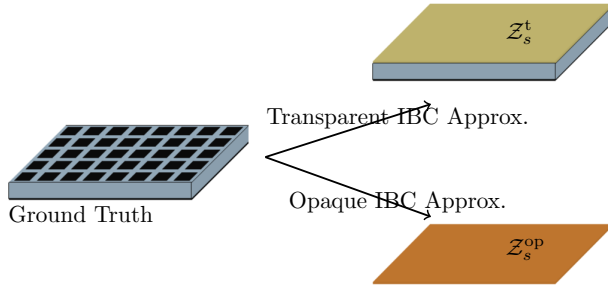


FIGURE 2. Transparent and Opaque IBC applied on a metasurface.

It is apparent that the transparent version has a higher degree of complexity and leads to a more accurate representation of the physical problem. However, the opaque version is convenient when modeling thicker structures terminated in a conducting plane (e.g., bed-of-nails).

The transparent IBC formulation considers both reflection and transmission of the fields through a surface by relating the average electric field to the jump of the magnetic field,

$$\hat{\mathbf{n}} \times \frac{1}{2}(\mathbf{E}_+ + \mathbf{E}_-) = \hat{\mathbf{n}} \times \underline{\underline{\mathcal{Z}}}_s (\hat{\mathbf{n}} \times (\mathbf{H}_+ - \mathbf{H}_-)) \quad (1)$$

On the other hand, the Opaque Impedance Boundary Condition solely considers the reflective component of a wave interacting with a surface; it relates the fields on one side using the opaque surface impedance $\underline{\underline{\mathcal{Z}}}_s^{op}$:

$$\hat{\mathbf{n}} \times \mathbf{E}_+ = \hat{\mathbf{n}} \times \underline{\underline{\mathcal{Z}}}_s^{op} (\hat{\mathbf{n}} \times \mathbf{H}_+) \quad (2)$$

While the opaque and transparent impedances are clearly different, when the bottom half space is a layered medium (possibly grounded) they can be approximately related to each other using the equivalent transmission line model of the layered medium.

B. EFIE-IBC INTEGRAL EQUATION

The integral equation associated with the structures of present interest is derived as usual via the equivalence theorem, with the addition of the surface impedance boundary condition (IBC) (in lieu of the PEC boundary condition) [11]. The background medium resulting from the application of the equivalence theorem is the free space for the opaque case, and a layered medium, possibly grounded, for the transparent case. For planar surfaces, the Integral Equation can be written in a unified form for both transparent and opaque IBC as

$$-\hat{\mathbf{n}} \times \hat{\mathbf{n}} \times \eta_0 \mathcal{L}(\mathbf{J})(\mathbf{r}) + \mathcal{Z}_s \cdot \mathbf{J}(\mathbf{r}) = -\hat{\mathbf{n}} \times \hat{\mathbf{n}} \times \mathbf{E}^{inc}(\mathbf{r}), \quad \forall \mathbf{r} \in \Gamma \quad (3)$$

where:

- $\mathbf{J} = \hat{\mathbf{n}} \times (\mathbf{H}_+ - \mathbf{H}_-)$ for the transparent case, and $\mathbf{J} = \hat{\mathbf{n}} \times \mathbf{H}_+$ for the opaque one;
- the impedance value \mathcal{Z}_s stands either for \mathcal{Z}_s^t in transparent cases, or $\mathcal{Z}_s^{op}/2$ for opaque ones;
- \mathbf{E}^{inc} is the field produced by independent sources in the background medium;

and

$$\mathcal{L}(\mathbf{X})(\mathbf{r}) = \int_{\Gamma} \underline{\underline{\mathcal{G}}}^{ej}(\mathbf{r} - \mathbf{r}') \cdot \mathbf{X}(\mathbf{r}') d\mathbf{r}' \quad (4)$$

is the Electric-Field Integral Operator (EFIO), in which $\underline{\underline{\mathcal{G}}}^{ej}$ is the Green's function of the background medium. For the opaque case, it is the Green's function of the upper homogeneous half-space, while, for the transparent case, it is that of the layered medium [19].

C. METHOD OF MOMENTS DISCRETIZATION

To numerically solve the EFIE-IBC (3), the planar surface Γ is discretized into triangular elements of average edge length h . The surface current \mathbf{J} is approximated as

$$\mathbf{J}^\Lambda(\mathbf{r}) = \sum_{n=1}^{N^\Lambda} j_n^\Lambda \mathbf{\Lambda}_n(\mathbf{r}),$$

where $\{\mathbf{\Lambda}_n\}$ indicates a set of Rao-Wilton-Glisson (RWG) basis functions [20] of N^Λ elements. By the Galerkin testing method applied to (3), we obtain the EFIE-IBC linear system

$$\mathbf{Z}^\Lambda \mathbf{j}^\Lambda = [\eta_0 \mathbf{L}^\Lambda + \mathcal{Z}_s \mathbf{G}^\Lambda] \mathbf{j}^\Lambda = \mathbf{e}^i \quad (5)$$

where \mathbf{j}^Λ collects the unknown coefficients, and

$$[\mathbf{L}^\Lambda]_{mn} = \langle \mathbf{\Lambda}_m; -\hat{\mathbf{n}} \times \hat{\mathbf{n}} \times \mathcal{L}(\mathbf{\Lambda}_n) \rangle \quad (6)$$

$$[\mathbf{G}^\Lambda]_{mn} = \langle \mathbf{\Lambda}_m; \mathbf{\Lambda}_n \rangle \quad (7)$$

$$[\mathbf{e}^i]_m = \langle \mathbf{\Lambda}_m; -\hat{\mathbf{n}} \times \hat{\mathbf{n}} \times \mathbf{E}^{inc} \rangle \quad (8)$$

where $\langle \mathbf{f}; \mathbf{g} \rangle = \int_{\Gamma} \mathbf{f}(\mathbf{r}) \cdot \mathbf{g}(\mathbf{r}) d\mathbf{r}$.

III. ANALYSIS OF EFIE-IBC ILL-CONDITIONING VIA EIGENVALUE SPECTRUM

In this paper, we will consider the simplest case of a spatially constant, scalar impedance. The above assumption is important to allow a theoretical analysis of the causes of

ill-conditioning, and to provide a solution to it. On the other hand, the ensuing approach described later on in Sec. IV.B is generally applicable, and consideration of its extension to non-constant impedance will be sketched in Sec. IV.E. To be specific, all numerical examples will refer to two reference structures, one for the opaque case and one for the transparent case.

- a) *Opaque Study Case.* The reference structure in this case is a rectangular plate, meshed with $N^\Lambda = 3472$ RWG (uniform mesh density $h \approx \lambda_0/17$), at a frequency of 18 GHz.
- b) *Transparent Study Case.* The reference structure in this case is a square plate, where the IBC sheet is above a grounded dielectric slab with dielectric constant $\epsilon_1 = 3\epsilon_0$, thickness 0.5 mm, with a meshed density $h \approx \lambda_1/20$ ($N^\Lambda = 4272$ RWG), where $\lambda_1 = \lambda_0\sqrt{3}$ is the substrate wavelength, at a frequency of 18 GHz.

We begin by analyzing the conditioning of the EFIE-IBC problem (5) as a function of the value of the surface impedance \mathcal{Z}_s . This is done in the present section through observation of the numerical results for the two study cases mentioned above; the reason of this behavior will be discussed in Sec. III.A.

The results are reported in Fig. 3 for the opaque case, and in Fig. 4 for the transparent one. It is apparent that capacitive values are safe, except for a narrow range corresponding to very large capacitance (small reactance). For typical, non-resonant sub-wavelength unit cells such values are unattainable, as can be seen in the examples reported in App. VI.B.

On the other hand, inductive surface impedance values are problematic, as the resulting condition number is generally large. For reference, the condition number for a PEC plate is on the order of 10^2 ; equally problematic is the fact that variations are erratic: the latter behavior is clear in the blow-up shown in the inset of Fig. 4. This erratic behavior is expected to be especially troubling when modelling modulated metasurfaces, thus with variable reactance values.

A. EIGENVALUE SPECTRUM ANALYSIS

The conditioning results described above are consistent with the findings in [11]; the present section is a point of departure from that work, providing an explanation in terms of the eigenvalue spectrum of the involved EFIE-IBC operator. This analysis is again based on the numerical study cases listed above, although in Sec. III.B it will be shown that the structure of the eigenvalue spectrum is indeed general.

As already mentioned, we consider a spatially constant, scalar impedance. The constant value of impedance allows retaining the convolutional nature of the EFIE kernel also in the EFIE-IBC: this allows analyzing the spectral properties of the involved operators, and obtaining a simple and meaningful link between the reactive loading and the spectrum.

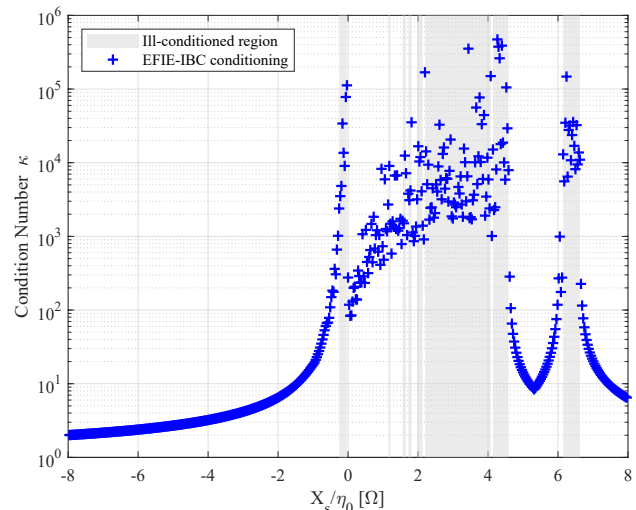


FIGURE 3. Condition number of the EFIE-IBC matrix for pure reactive impedance values $\mathcal{Z}_s = j\mathcal{X}_s$, opaque impedance. The plate is $3\lambda_0 \times 1\lambda_0$, with uniform mesh $h \approx \lambda_0/17$ ($N^\Lambda = 3472$), illuminated at 18 GHz.

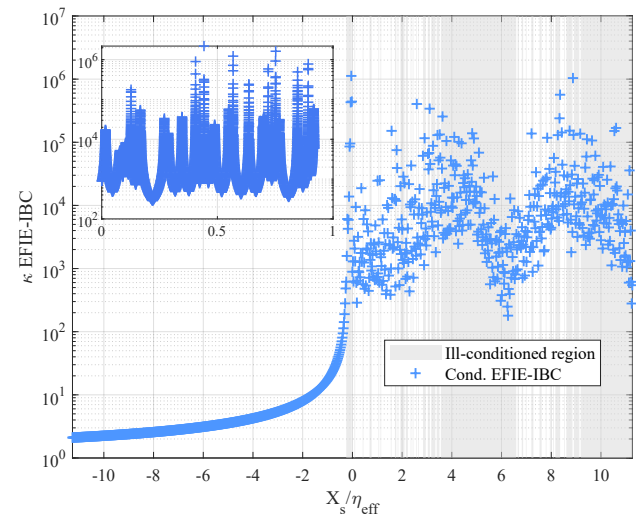


FIGURE 4. Condition Number of the EFIE-IBC matrix problem on a $1\lambda_0 \times 1\lambda_0$ plate for transparent scalar IBC $\mathcal{Z}_s = j\mathcal{X}_s$ meshed by $N^\Lambda = 4272$ RWG; the background medium is a grounded dielectric substrate, with $\epsilon_d = 3\epsilon_0$ and thickness $d = 0.5$ mm.

In fact, the ill-conditioning of the system may be a symptom of an ill-posed problem, and thus it is relevant to investigate the properties of the operators appearing in the formulation. We begin by analyzing the properties of the EFIE operator appearing in the EFIE-IBC (3), as the properties of this operator are well known; next, we will analyze the impact of the IBC term on that spectrum. We recall that the EFIE operator is the one pertinent to a PEC, to which the EFIE-IBC reduces for $\mathcal{Z}_s = 0$.

The eigenvalue problem for the continuous operator reads

$$\mathcal{L}(\phi_i)(\mathbf{r}) = \zeta_i \phi_i(\mathbf{r}) \quad (9)$$

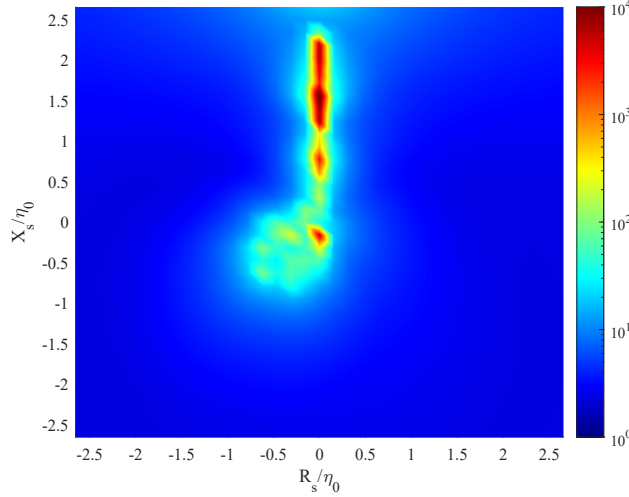


FIGURE 5. Ill-conditioning of the EFIE-IBC formulation on a rectangular plate of size $3\lambda_0 \times 1\lambda_0$ with a uniform mesh $h \approx \lambda_0/9$ ($N^\Lambda = 895$). The plot shows the condition number as a function of the impedance value $\mathcal{Z}_s = R_s + j\mathcal{X}_s$.

and its discretization with the RWG basis

$$\phi_i(\mathbf{r}) = \sum_{n=1}^{N^\Lambda} \varphi_{i,n} \mathbf{\Lambda}_n(\mathbf{r}),$$

yields the generalized matrix eigenvalue problem

$$\eta_0 \mathbf{L}^\Lambda \varphi_i = \zeta_i \mathbf{G}^\Lambda \varphi_i \quad (10)$$

On the other hand, the eigenproblem for the continuous EFIE-IBC operator is

$$\mathcal{L}(\phi'_i)(\mathbf{r}) + \mathcal{Z}_s \phi'_i(\mathbf{r}) = \zeta_i^Z \phi'_i(\mathbf{r}) \quad (11)$$

and comparison with (9) yields immediately $\phi'_i(\mathbf{r}) = \phi_i(\mathbf{r})$, and

$$\zeta_i^Z = \zeta_i + \mathcal{Z}_s \quad (12)$$

which clearly shows that for reactive surfaces the IBC term $\mathcal{Z}_s = j\mathcal{X}_s$ results in *shifting along the imaginary axis the eigenvalues of the EFIE*, i.e., those for the case of a PEC surface. As we will see, this property will prove crucial in assessing the posedness of the EFIE-IBC.

We now analyze the eigenspectrum of the EFIE (i.e., for a PEC surface). For the current analysis, the properties of the EFIE for a layered medium can be considered equivalent to those for a free-space kernel. The EFIE appears as a first kind Fredholm integral equation [21], and a superficial analysis could lead to considering it ill-posed. However, it has been shown that the EFIE operator effectively acts as a second kind Fredholm operator [22], [23], ensuring its well-posedness, thanks to the singularity of its kernel. This can be appreciated by the EFIE eigenvalue spectrum in Fig. 6, in which we have employed the generalized eigenvalues to show those of the operator, and for uniformity with the EFIE-IBC case; as seen there, the PEC \mathbf{Z}^Λ matrix shows non-zero eigenvalues with a clear gap around the origin. As expected, a very similar situation holds for the EFIE in presence of a grounded dielectric, as shown in Fig. 7.

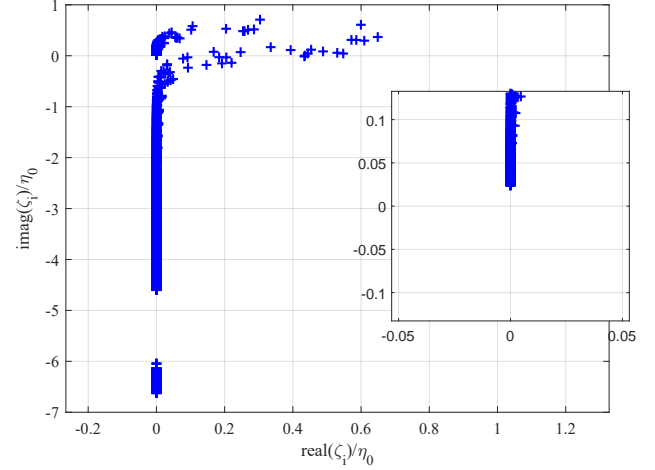


FIGURE 6. Generalized Eigenvalues distribution of the continuous EFIE operator \mathcal{L} in free-space (relative to opaque case), normalized by the free-space intrinsic impedance η_0 , for a $3\lambda_0 \times 1\lambda_0$ plate with mesh density $h \approx \lambda_0/17$.

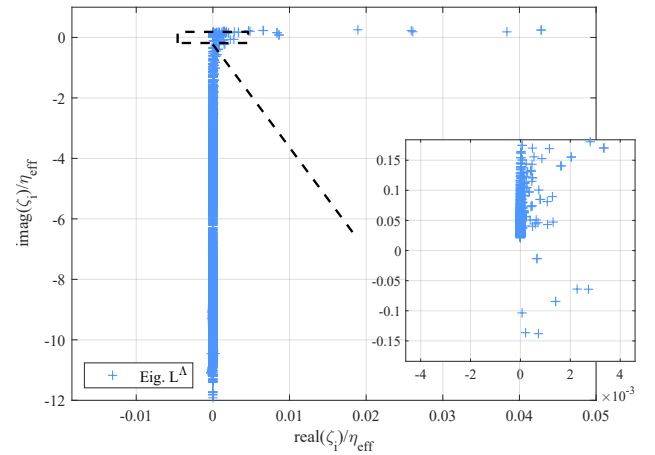


FIGURE 7. Generalized Eigenvalues distribution of the continuous EFIE operator \mathcal{L} in presence of a grounded dielectric slab, normalized by the “effective” intrinsic impedance η_{eff} , for a $1\lambda_0 \times 1\lambda_0$ plate illuminated at 18 GHz. The plate is uniformly meshed with $h \approx \lambda_d/20$.

In the eigenvalue spectrum we can notice two separated branches: the “inductive” branch with $\Im(\zeta) > 0$ corresponds to solenoidal eigenfunctions, and the “capacitive” one to (weakly) irrotational eigenfunctions [24], [25].

We recall that the condition number (in 2-norm) is the ratio between the maximum and minimum eigenvalues,

$$\kappa = \frac{\zeta_{\text{max}}}{\zeta_{\text{min}}} \quad (13)$$

and a large condition number results when an eigenvalue approaches zero, which in our case corresponds to critical eigenvalues ζ_c^Z for which

$$\zeta_c^Z \approx 0 \rightarrow \mathcal{Z}_s \approx -\zeta_c \quad (14)$$

This is seen by comparing Fig. 5 with Fig. 6: the peaks of κ in Fig. 5 indicate the values for which the conditions (14) applies, i.e., $\mathcal{Z}_s \approx -\zeta_c$.

In particular, one is interested in passive, lossless surface impedances, i.e., purely imaginary,

$$\mathcal{Z}_s = j\mathcal{X}_s.$$

This results in shifting the eigenvalues along the imaginary axis, potentially filling the gap around zero seen in Fig. 6; this is exemplified in Fig. 8. It is thus apparent that the *sign* of the reactance \mathcal{X}_s , i.e., its capacitive or inductive nature, plays a key role in this.

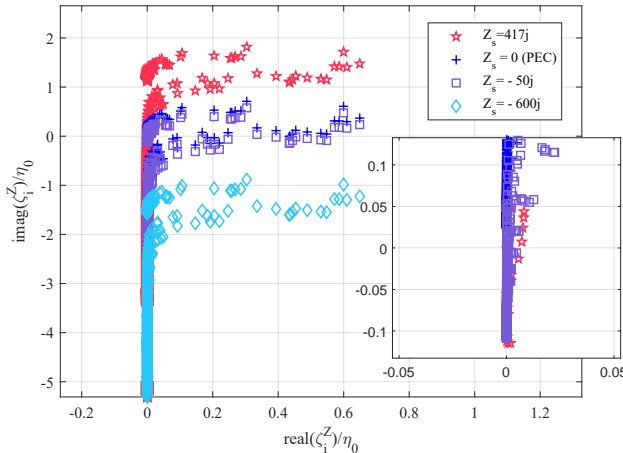


FIGURE 8. Generalized Eigenvalues distribution of the operator $\mathcal{L} + \mathcal{Z}_s \mathcal{I}$ for the opaque case, considering different impedance values, illustrating the eigenvalues shift due to IBC addition. Results obtained for a $3\lambda_0 \times 1\lambda_0$ plate with mesh density $h \approx \lambda_0/17$. The eigenvalues are normalized by η_0 .

This analysis indicates that the ill-conditioning appearing for certain ranges of reactances is *intrinsic* to the EFIE-IBC operator itself, and as such is not related to its discretization. Hence, solutions to possible ill-conditioning should start from this consideration. The property of the operator translates into an ill-conditioning of the matrix system that may depend on the discretization, as the latter may affect the numerical eigenvalues, e.g., their number, and specific values. As a result, the addition of the IBC term in (3) may shift imaginary eigenvalues closer or less close to zero, and this in turn will affect the condition number. This explains the (erratic) peaks in Figs. 3-4: for a given structure, eigenvalues are a discrete set, and a continuous variation of reactance generates different eigenvalues to successively get close to zero, thus generating peaks in the condition number.

As in typical applications the impedance will be spatially varying (“modulated”), it is apparent that the regularization scheme must be such as to cover all possible instability sources.

Before proceeding further into the analysis, we show the situation for the case of a dielectric slab backed by a (“ground”) metal plane. This is typical in metasurface antennas with on-surface feeding, and in reflective metasurfaces (e.g., RIS); the ground is absent in transmissive metasurfaces (e.g., metalenses). We concentrate here on the grounded case for breadth, as it is the most different from the free space

case. The relevant graphs are in Fig. 4 and 7. One can note that the dependence of the condition number is oscillating faster than in the opaque/free-space case, making it more difficult to predict safe zones. There are also differences in the distribution of the eigenvalues in the complex plane (Fig. 7), and in particular the reduced gap between irrotational and solenoidal branches around the origin.

As clear from Fig. 3 and 5, there are two instability branches: one for positive (inductive) values of reactance, and one for negative (capacitive) ones. The latter appears for very small values of $|\mathcal{X}_s|$, which correspond to a very large capacitance; as such, for sub-wavelength unit cells this regime is usually outside of the range typically encountered in practice (see also App. VI.B). The possible physical origin of this is beyond the scope of this paper; we note however that the IBC is an approximation, and no guarantee of unconditional stability can be assumed.

One important consideration is that the numerical ill-conditioning appears to be part of the *model equation* (the EFIE-IBC), not an artifact of its numerical solution. Crucially, the possible appearance of (one or more) null eigenvalues indicates that the EFIE-IBC model equation may not be well-posed.

Ill-conditioning typically manifests in the form of a) slow, stagnating, or absent convergence of iterative solvers, and/or b) noisy solutions. It is important to note that even when the effects of the ill-conditioning are avoided in the numerical solution, the “right” solution to the problem (as formulated with the EFIE-IBC) may not exist without appropriate stipulations—essentially, of how to exclude the null space associated to the problematic eigenvalues. This situation is very different from, e.g., the dense-mesh ill-conditioning of the well-posed EFIE (PEC), where a “right” solution exists, and the task is to construct numerical schemes (pre-conditioners) that are able to get it.

This means that the practical approach to get a stable result for the EFIE-IBC in critical cases is a *regularization* procedure based on the insertion of a priori information on the property of the desired solution.

On the other hand, the ill-posedness (or less critically, the ill-conditioning) is a property of the continuous EFIE-IBC operator; hence, the assessment of the *range* of potentially unstable values can be done by considering a “sample” of the overall (possibly large) structure. This means that all the related steps will have a fractional numerical cost.

B. GENERAL SHAPE OF EIGENVALUE SPECTRUM

As discussed in the previous section III, the distribution of the eigenvalues of the EFIE in the complex plane plays a fundamental role in the well-posedness issue of the EFIE-IBC.

For the sake of conciseness, we will adopt the terminology *shape of the eigenvalue spectrum* (or its shorthand shape of the eigenspectrum) to refer to the distribution of the eigenvalues (of the EFIE-IBC or EFIE) in the complex plane.

In the preceding discussion, the shape of the eigenspectrum had been obtained “experimentally” from the numerical analysis of specific cases. In this section, we show that the observed shape is indeed the general shape.

The strategy of this analysis is the following: as the matrix system has a real part that is much smaller than its imaginary part, we can therefore discuss the spectrum using the classical results of eigenvalue perturbation [26]. Two further results will also shed light on this spectrum. Under Galerkin testing, the system matrix is symmetrical (yet not Hermitian) due to reciprocity: this impacts on the eigenvectors, and will allow to separate real and imaginary parts of the eigenvalues. Second, the real part of the matrix is due to radiation, and radiation happens only for components with spatial frequency in the visible range.

We begin by explicitly writing the EFIE (generalized) eigenvalue problem:

$$\eta_0 \mathbf{L}^\Lambda \varphi = \zeta \mathbf{G}^\Lambda \varphi. \quad (15)$$

The EFIE matrix is now written as

$$\mathbf{L}^\Lambda = \mathbf{R} + j\mathbf{X}, \quad (16)$$

and reciprocity and Galerkin testing result in

$$\mathbf{L}^{\Lambda T} = \mathbf{L}^\Lambda, \quad \mathbf{R}^T = \mathbf{R}, \quad \mathbf{X}^T = \mathbf{X}. \quad (17)$$

Using

$$\|\mathbf{R}\|_2 \ll \|\mathbf{X}\|_2 \quad (18)$$

we consider the original eigenvalue problem (10), (15) as perturbation of the same for the imaginary part only,

$$\eta_0 \mathbf{X} \varphi^{(0)} = \xi^{(0)} \mathbf{G}^\Lambda \varphi^{(0)}. \quad (19)$$

Due to symmetry, $\xi^{(0)}$ are real, and the eigenvectors $\varphi^{(0)}$ are real and form an orthogonal basis

$$\langle \varphi_m^{(0)}, \varphi_n^{(0)} \rangle = \delta_{m,n}, \quad (20)$$

where we have defined

$$\langle \mathbf{u}, \mathbf{v} \rangle = \mathbf{u}^T \mathbf{G}^\Lambda \mathbf{v}. \quad (21)$$

Relating the unperturbed problem (19) to the original one (10) through the Matrix Perturbation Theory at the first order [26], and considering the RWG Gram Matrix \mathbf{G}^Λ being unperturbed since only related to the mesh, we can express the eigenvalues as

$$\zeta_m \approx j\xi_m^{(0)} + \delta\zeta_m \quad (22)$$

where the perturbation $\delta\zeta_m$ is reduced to the simple case

$$\delta\zeta_m = \langle \varphi_m^{(0)}, \mathbf{R} \varphi_m^{(0)} \rangle. \quad (23)$$

Thus, $\delta\zeta_m$ is real and will be henceforth called $\rho_m = \delta\zeta_m$.

Since the term $\mathbf{R} \varphi_m^{(0)}$ represents the radiation contribution of the function $\varphi_m^{(0)}$, the real perturbation term ρ_m is non-negligible only for $\varphi_m^{(0)}$ having spatial frequency contents not much higher than k_0 , whereas faster variations are responsible for the purely imaginary eigenvalues. This is slightly modified in the case of a dielectric background (transparent case), as the “radiative” region of the wavenumber spectrum has to be enlarged up to $k_{\text{eff}} = \sqrt{\frac{\epsilon_r d + 1}{2}} k_0$ to include active power coupling into possible guided wave modes in the slab.

IV. REGULARIZATION

A. WAVENUMBER ANALYSIS OF EIGENVALUE SPECTRUM AND REGULARIZATION

Based on the above results, we now analyze the PEC EFIE eigenvalue spectrum regarding the wavenumber spectrum content of their associated eigenfunctions. As the eigenfunctions $\phi_m(r)$ associated to the eigenvectors $\varphi_m^{(0)}$ are orthogonal and have spatial support over the entire structure (unlike the spatially-localized RWGs) they are highly localized in the Fourier Transform domain (k_x, k_y) , in a manner similar to waveguide mode basis functions to be discussed later on in Sec. IV.B. We then track the wavenumber plane position $(k_x, k_y)_i^{\text{peak}}$ where the eigenfunction associated to the i -th eigenvalue has its peak, and we consider $k_{\rho i}^{\text{peak}} = \sqrt{(k_x^2 + k_y^2)_i^{\text{peak}}}$.

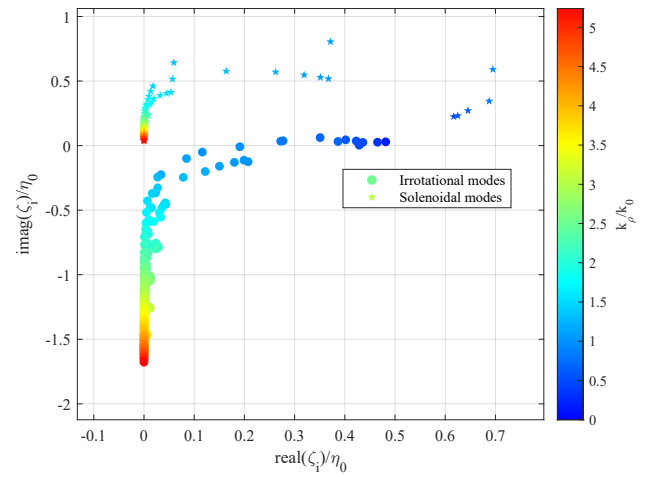


FIGURE 9. Generalized Eigenvalues distribution (from Figure 6) with their wavenumber spectrum peak $k_{\rho i}^{\text{peak}}$ (obtained with the approximate method in Sec. IV.B). Free-space EFIO operator (opaque case)

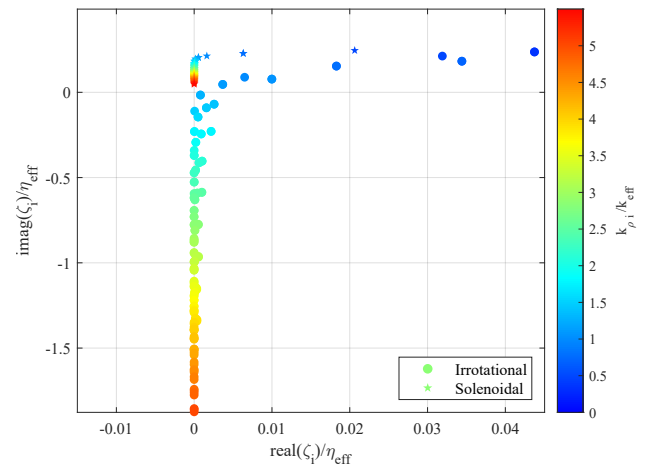


FIGURE 10. Generalized Eigenvalues distribution with their wavenumber spectrum peak $k_{\rho i}^{\text{peak}}$ (obtained with the approximate method in Sec. IV.B). Grounded dielectric slab EFIO operator (transparent case)

Next, we graphically attach this wavenumber spectrum information to the EFIE eigenvalues, as shown in Figs.

9 and 10. The two branches of the eigenvalue spectrum have opposite wavenumber spectrum behaviors: the positive (inductive) branch has the smallest eigenvalue associated to the lowest spectral content, while the opposite is seen for the other branch.

This analysis indicates a possible regularization scheme: exclude portions of the wavenumber spectrum that correspond to problematic EFIE PEC eigenvalues ζ_c that are pushed close to zero (or to zero) by the addition of the IBC reactance. This is possible if one can control the spatial variation of the employed basis functions; we will see this can be done by retaining the RWG system but effecting a *filtering*, as described in Sec. IV.B.

We now pass to finding a practical way of determining what wavenumber components have to be filtered out, leaving the discussion on how to implement this filtering to Sec. IV.B. This will be done by using the previously discussed link between EFIE eigenvalues ζ_i and the wavenumber spectrum content $k_{\rho i}^{\text{peak}}$ of their associated eigenfunctions ϕ_i . Hence, it is important to stress that it will not be necessary to actually compute that eigenspectrum, which would make the approach unfeasible for practical sizes of the problem. We will see that a wise choice of basis function will avoid most of that numerical burden. The concerned figures 9, 10, 11, and 12 have indeed been obtained directly by that approximate method.

This discussion is aided by concentrating on the imaginary subset of the eigenspectrum, i.e., by displaying only the EFIE eigenvalues ζ_i that have zero or (numerically) negligible imaginary part. In fact, only these can become null or near-zero eigenvalues of the EFIE-IBC $\zeta_i^Z = \zeta_i + j\mathcal{X}_s$ for reactive IBC surfaces. This is graphically reported in Figs. 11 and 12. In them, the abscissa indicates the imaginary part of the eigenvalue, $\Im(\zeta_i)$, and the ordinate the wavenumber plane peak $k_{\rho i}^{\text{peak}}$ of its associated eigenfunction ϕ_i . Hence, a vertical line $\Im(\zeta_i) = -\mathcal{X}_s^c$ will indicate the IBC value that “kills” the eigenvalue $\zeta_{ic}^Z = \zeta_{ic} - j\mathcal{X}_s^c$ corresponding to the intersection with the reported curves (note sign reversal for ease of visualization). Using the method described in [27] for spectrally localized basis functions, one can show that the $\Im(\zeta_i) \leftrightarrow k_{\rho i}^{\text{peak}}$ mapping is monotonous above $k_F > k_0$, as indeed seen in the related figures.

To avoid the ill-posedness associated with EFIE-IBC eigenvalues zeroing, it would be sufficient to avoid basis functions with wavenumber spectra peaking close to the critical $k_{\rho i,c}^{\text{peak}}$ value. We will take a more conservative and simpler choice, keeping only the basis functions for which their associated $k_{\rho i} < k_{\rho i,c}^{\text{peak}}$; the counterpart of it, will be referred to as the “Inaccessible Wavenumber Spectrum”, i.e., spectral region not covered by the employed basis functions. Figures 11 and 12 illustrate this idea, where the gray zone $k_{\rho} > k_{\rho i,c}^{\text{peak}}$ indicates the IWS.

One could object that deleting only a few wavenumber values around $k_{\rho i,c}^{\text{peak}}$ would be enough to regularize the problem. This could be the case if one has precise information about

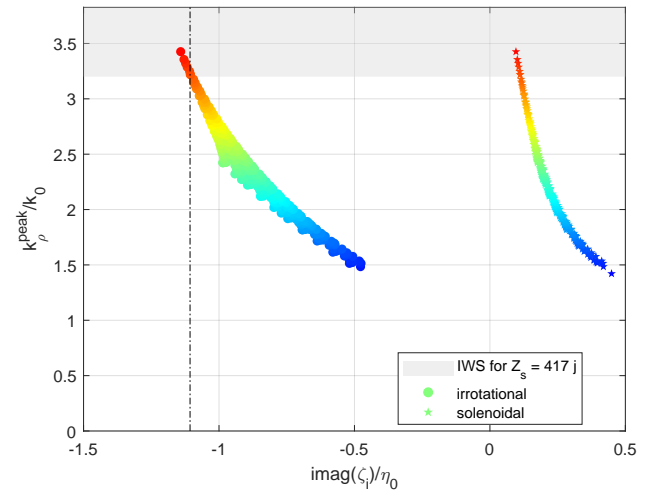


FIGURE 11. Wavenumber spectrum of the subset of the generalized eigenvalues that are purely imaginary. The gray zone indicates the *Inaccessible Wavenumber Spectrum (IWS)* for the opaque $Z_s = 417j$ value indicated by the dashed line. The Z_s value used here is the one presented in Sec. V.D. The markers are colored as in Figs. 9–10 for ease of reference.

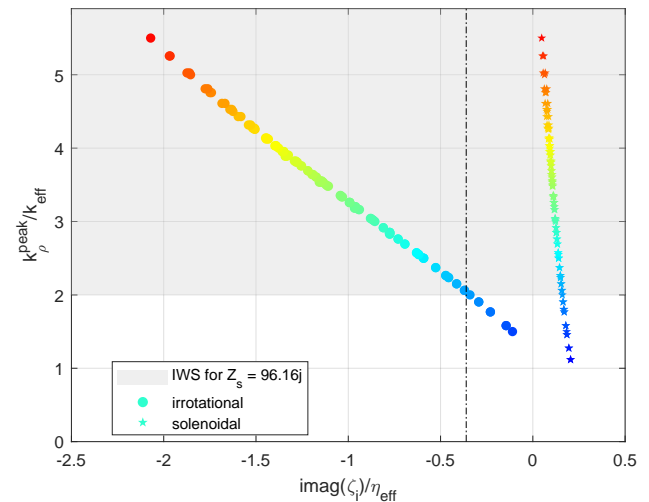


FIGURE 12. Wavenumber spectrum of the subset of the generalized eigenvalues that are purely imaginary. The gray zone indicates the *Inaccessible Wavenumber Spectrum (IWS)* for the transparent $Z_s = 96.16j$ value indicated by the dashed line. The Z_s value used here is the one presented in Sec.V.E. The markers are colored as in Figs. 9–10 for ease of reference.

the mapping, i.e., relying too much on the approximation. Furthermore, we are not able at this time to assign a precise “physical” meaning to this choice, and we did not pursue this option further.

On the other hand, the proposed strategy is a low-pass filtering option with well-known properties. In the following, we will indicate the largest allowed wavenumber peak as k_F and label it with the term “cut-off wavenumber”.

Finally, we recall that the regularization analysis above only involves the problematic IBC values, i.e., (essentially) inductive ones. Also, note that impedance values corresponding to the imaginary parts of the eigenvalues are not

problematic as long as the real part of these eigenvalues is non-negligible. This “safe zone” for the impedance \mathcal{X}_s is therefore not present in Figs. 11 and 12.

B. WAVENUMBER FILTERING IMPLEMENTATION

We have seen that regularization of the EFIE-IBC can be achieved by excluding the Inaccessible Wavenumber Spectrum. This can be implemented using several approaches; of most relevance are the implementations based on selecting basis functions with appropriate properties. Ideally, our best basis functions would be the EFIE eigenfunctions; however, what we actually need of them is the ability to resolve the wavenumber spectrum, i.e., that they can be organized in subsets such that the spectra are localized in different portions of the wavenumber spectrum. For example, RWG functions are the opposite: they resolve the space (are non-zero only on pairs of triangles), and their Fourier Transform are essentially all equal. When available, waveguide modes are a good example of spectrally resolved basis functions, as evident in the case of rectangular domains. Intermediate versions, suitable for general shapes, are hierarchic multi-resolution basis functions [27], [28]. In the following, we will use the term “Spectral Basis Functions” (SBF) to indicate spectrally-resolved sets of basis functions.

As practical metasurfaces have most often a contour of simple shape, we will use waveguide modes in the following; as they are orthogonal and all have the same spatial domain, their wavenumber spectra will be maximally localized, with important features for the present analysis. We observe that the direct generalization of waveguide modes for general polygonal shapes are the basis functions described in [29]; for these basis functions, the use in conjunction with fast factorizations as in [30] is direct.

C. WAVEGUIDE MODES BASIS FUNCTIONS

We consider the modal eigenfunctions $\Phi_i(\mathbf{r})$ of a waveguide with perfectly magnetic conductor (PMC) boundary conditions; they represent div-conforming basis functions well suited to discretize the EFIE operator [27], [28], [30]. With these, we approximate the unknown current as,

$$\mathbf{J}(\mathbf{r}) \approx \mathbf{J}^\Phi(\mathbf{r}) = \sum_{i=1}^{N^\Phi} j_i^\Phi \Phi_i(\mathbf{r}), \quad (24)$$

where the subscript $i = (m, n)$ stands for the (m, n) -th mode. The basis functions are expressed as a linear combination of RWG, which allows, inter alia, to reuse all existing codes for general geometries, i.e.,

$$\Phi_i(\mathbf{r}) = \sum_{n=1}^{N^\Lambda} \Phi_{n,i} \Lambda_n(\mathbf{r}). \quad (25)$$

The coefficients of the RWG representation are computed from the analytical expression of the modal basis functions in App. VI.A by the weighted residual method as in [30],

resulting in

$$\langle \Lambda_m; \Phi_i \rangle = \sum_{n=1}^{N^\Lambda} \Psi_{ni} \langle \Lambda_m; \Lambda_n \rangle \quad \forall m \in 1, \dots, N^\Lambda \quad (26)$$

Equation (26) is equivalent to the matrix problem,

$$\mathbf{G}^\Lambda \boldsymbol{\Psi}_i = \begin{bmatrix} \langle \Lambda_1; \Phi_i \rangle \\ \vdots \\ \langle \Lambda_{N^\Lambda}; \Phi_i \rangle \end{bmatrix} \quad (27)$$

where $\boldsymbol{\Psi}_i$ is the i -th column of the matrix $\boldsymbol{\Psi}$, which represents the basis change between the RWG and the SBF spans. The linear system 27 above can be solved at low cost since the RWG Gram matrix is positive-definite and with conditioning of $\mathcal{O}(1)$ (an iterative solution converges in $\mathcal{O}(1)$ iterations).

Using the Spectral Basis, the EFIE-IBC linear system (5) becomes

$$\mathbf{Z}^\Phi \mathbf{j}^\Phi = \boldsymbol{\Psi}^T \mathbf{e}^i, \quad \mathbf{Z}^\Phi = \boldsymbol{\Psi}^T \mathbf{Z}^\Lambda \boldsymbol{\Psi}. \quad (28)$$

Finally, (25) into (24) yields the Spectral Basis solution directly in terms of RWG,

$$\mathbf{J}^\Phi(\mathbf{r}) = \sum_{n=1}^{N^\Lambda} j_n^{\Lambda\Phi} \Lambda_n(\mathbf{r}), \quad j_n^{\Lambda\Phi} = \sum_{i=1}^{N^\Phi} \Phi_{n,i} j_i^\Phi \quad (29)$$

or

$$j^{\Lambda\Phi} = \boldsymbol{\Psi} \mathbf{j}^\Phi.$$

A very relevant property of the spectral basis is its close resemblance to the eigenfunctions of the EFIE, $\phi_i(\mathbf{r})$, which makes the diagonal of the system matrix in this basis very close to the eigenvalues ζ_i , as observed in Fig. 13. (An approximate explanation of this property can be found in [27]). This has two positive consequences:

- The inverse of the diagonal of the system matrix in the SBF affords a potent preconditioner of that matrix, as seen in Tab. 1 and 2; this will be used in the following.
- As the diagonal entries of the matrix are a close approximation of the actual eigenvalues, the entire regularization process described in Sec. IV.A can be carried out without additional numerical cost.

D. FILTERING METHOD COMPUTATIONAL COST

Computational complexity is an obvious numerical issue in all simulation and design methods. As we will discuss here, the regularization filtering often comes at a cost, and therefore it is important to put it in perspective.

The use of spectral basis functions may actually accelerate the *optimization* process (i.e., design), as discussed in [30], while requiring a higher cost for a *single* analysis (simulation). The perspective here however is different: when dealing with problematic (inductive) impedance values, one is facing a possibly ill-posed model problem, and the key issue is having a reliable solution altogether. In this perspective, the numerical cost is important to assess the feasibility of the

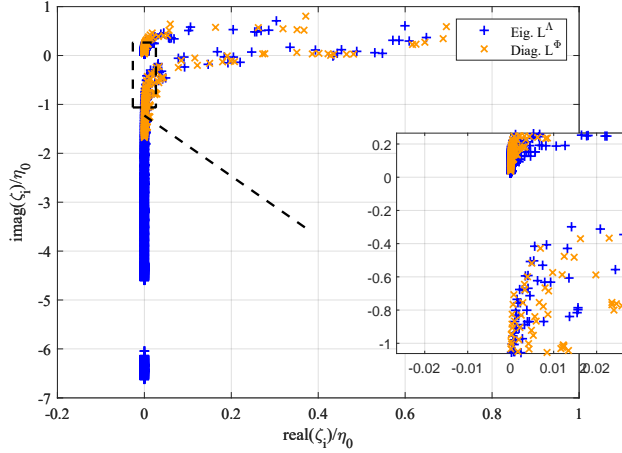


FIGURE 13. Comparison of the Generalized Eigenvalues distribution of the EFIE operator and the diagonal entries of the system matrix in the SBF basis, opaque case (free space).

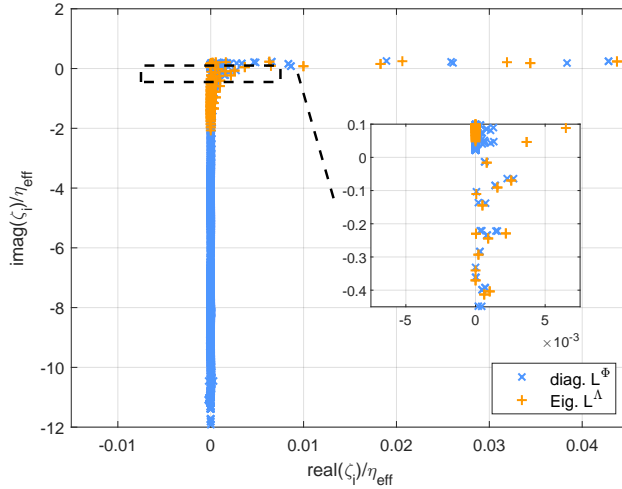


FIGURE 14. Comparison of the Generalized Eigenvalues distribution of the EFIE operator and the diagonal entries of the system matrix in the SBF basis, transparent case.

solution—not the possible advantage regarding a standard solution.

We will now address the computational cost estimation; the analysis draws from the similar exercise in [30] and [31]. In doing the analysis, we will follow the computational workflow in Fig. 15

The summary is that the filtering process has an overhead in constructing the system matrix $\mathbf{Z}^\Phi = \Psi^T \mathbf{Z}^\Lambda \Psi$ in (27), while possibly reducing the cost of the solve phase. The latter may be attained in two different manners: a) if employing a direct solver (e.g., LU), the reduction is due to a reduction of the number of unknowns as $N^\Phi < N^\Lambda$ (often in practice $N^\Phi \ll N^\Lambda$) due to the regularization effect; b) if using an iterative solver, the number of iterations is strongly reduced by the preconditioning effect of the basis (see Sec. V), also in the case of non-problematic values.

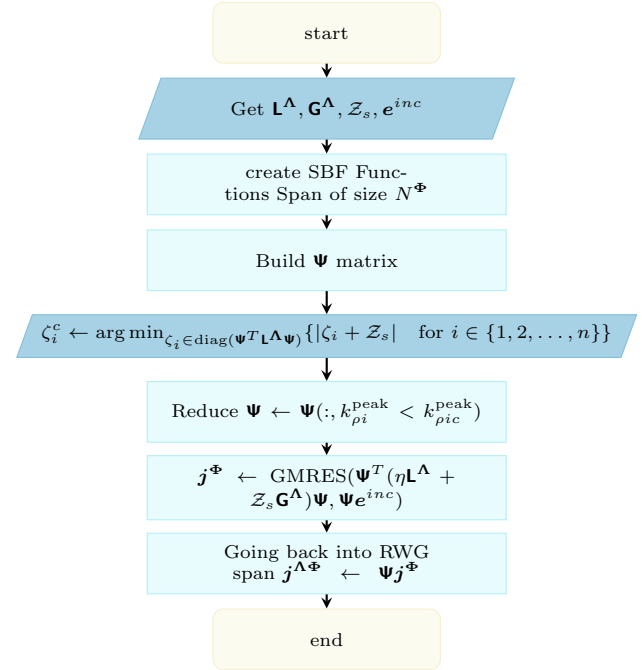


FIGURE 15. Filtering Algorithm Flowchart detailed in Sec. IV

1) BASELINE MOM

We start with the case of using a baseline MoM, i.e., without fast factorizations. The construction of the Ψ matrix as detailed in (27) has an overall cost of $\mathcal{O}(N^\Phi N^\Lambda)$; in fact, the RWG Gram Matrix is highly sparse, with a condition number close to one, so the associated linear system is iteratively solved with cost $\mathcal{O}(N^\Lambda)$ [32].

Then, we need to consider the construction and the solution of the new matrix problem in (28): the creation of the matrix \mathbf{Z}^Φ is a double matrix product with a cost of $\mathcal{O}(N^\Phi N^\Lambda^2)$, while retrieving the solution $j^\Lambda \Phi$ is a standard matrix-vector computation ($\mathcal{O}(N^{\Phi^2})$). The last remaining step is to solve the matrix problem, either by a direct method, like the LU inversion, with a complexity in $\mathcal{O}(N^{\Phi^3})$ or an iterative one; in this case, the time computation cost would be of $\mathcal{O}(n_{it}^\Phi N^{\Phi^2})$, where n_{it}^Φ is the number of iterations needed to reach the solution.

In the end, it means that the overall time computation cost of the filtering method is in $\mathcal{O}(N^\Phi N^\Lambda^2)$. As we have assured that $N^\Phi < N^\Lambda$, this is more advantageous than the standard EFIE-IBC computation cost; indeed, for impedance values in the ill-conditioning range (albeit where the problem is not ill-posed), the number of iteration n_{it} for a standard iterative solver (such as the Generalized Minimal Residual method (GMRES)) will make the cost equal or larger to the one of the direct LU inversion $\mathcal{O}(n_{it} N^\Lambda^2) \approx \mathcal{O}(N^\Lambda^3)$.

2) FAST FACTORIZATIONS

When using fast factorizations, like FFT, MLFMA, the cost of a matrix-vector product (matvec) scales (asymptotically)

as $\mathcal{O}(N \log N)$, where N is the matrix size. Following the analysis in [30], [31], if one uses a direct solver, the complexity of building the system matrix $\mathbf{Z}^\Phi = \Psi^T \mathbf{Z}^\Lambda \Psi$ of (27) scales as $\mathcal{O}(N^\Phi N^\Lambda \log N^\Lambda)$; the rest of the complexity analysis remains as in the baseline MoM.

For an iterative solver, the matvec $\mathbf{Z}^\Phi \mathbf{j}^\Phi = \Psi^T \mathbf{Z}^\Lambda \Psi \mathbf{j}^\Phi$ can be done first as $\mathbf{w} = \Psi \mathbf{j}^\Phi$ with complexity $\mathcal{O}(N^\Lambda N^\Phi)$ and then as $\Psi^T \mathbf{Z}^\Lambda \mathbf{w}$ with complexity $\mathcal{O}(N^\Phi N^\Lambda \log N^\Lambda)$, i.e., globally as $\mathcal{O}(N^\Phi N^\Lambda \log N^\Lambda) \approx \mathcal{O}(N^\Phi N^\Lambda)$. This approach has the additional advantage of not requiring full storage of the system matrices \mathbf{Z}^Λ and \mathbf{Z}^Φ .

E. EXTENSION TO MODULATED IMPEDANCE

The purpose of this work is primarily discussing the intimate nature of the EFIE-IBC instability and conveying two main messages: 1) the nature of the problem is ill-posedness, requiring a regularization, and a generic preconditioner is not guaranteed to solve the actual problem; 2) Wavenumber spectrum limitation has the ability to make the problem well-posed. However, it is possible to indicate how to use this approach in the more general case of non-constant impedance. How to implement that is, however, beyond the scope of the present communication.

The filtering can be done in various ways (see below) and not necessarily using modal basis functions; the latter are however well suited to canonical shapes (rectangle, circle, circle with hole, etc.) that are practical for many metasurface designs. Use of modal basis function has indeed already been reported for modulated metasurfaces [30].

The key issue is the choice of cut-off wavenumber k_F . We recall that our analysis is based on the eigenspectrum of the EFIE, i.e., for a PEC. Hence, in presence of a variable impedance the above analysis can be done by localization, i.e., by considering the range of impedance values, and for each of them assessing the possible problematic wavenumber range. With the union of all Inaccessible Wavenumber Spectra, one retains the most conservative value of the cut-off wavenumber k_F .

A more complicated issue is tensor impedance. While this is entirely outside the scope of this work, a simple consideration can guide the choice of the cut-off wavenumber k_F . One can consider the two eigenvalues of the tensor separately, treating each as a scalar and then adopting the most conservative choice.

V. NUMERICAL RESULTS

A. TESTING METHODOLOGY

In this section, we will first show that the proposed spatial filtering does not worsen the solution when the impedance renders the EFIE-IBC problem well-posed—i.e., for capacitive values. This is done for consistency, while not necessary in that case (while it might be advantageous for efficiency, as described in [30]); otherwise said, one can safely employ it in all cases.

Then we will address the issue of testing our proposed approach when the standard EFIE-IBC solution is unreliable. This testing requires a specific methodology: we have shown that in critical condition the EFIE-IBC problem is ill-posed, and the EFIE-IBC model as such is not a good model of the metasurface structures it aims to approximate. This means that even if the solution process converges, and even if the solution does not show obvious signs of ill-conditioning (as was the case for the noisy solutions reported in [11]), still there is no guarantee that the solution to that specific model problem is a good representation of the physics it purports to represent.

Because of this, we will start from a physical metasurface structure, which is what the IBC approximation aims to approximate. We then model it as an IBC, and check the results of EFIE-IBC *against those for the physical structure*. This way there will be no doubt as to the results (of course, within the margins of the IBC approximation of the physical structure).

The results for the reference physical structures will be labeled “ground truth” in the following. We have selected a structure to test the opaque case and one for the transparent (sheet) atop a grounded dielectric slab; they will be labeled according to the corresponding IBC model. We have chosen to excite the structure with a plane wave because that is expected to be the case where the ill-posedness is less visible, and thus most significant. In fact, an excitation in the visible wavenumber spectrum minimally projects on eigenfunctions (ϕ_i) associated to the most problematic eigenvalues of the EFIE-IBC.

With our normalization of operators, the eigenvalues have the physical dimensions of impedance (hence measured in Ohm); in order to simplify notations, the Ohm units in the following are implied and omitted; the same convention is used also for surface impedance values.

B. REFERENCE STRUCTURES

All the impedance values used in this section have been computed with the approximate expression from [33] and verified via full-wave simulation (periodic) on CST Studio [34] with the Sheet Extraction Method [35]; this ensures accurate IBC modeling of the reference structures.

1) Reference structure for opaque IBC test

The structure involves a capacitive impedance sheet, but it becomes inductive as an opaque IBC; this is typical in metasurface antennas with on-surface feeding, which involve a TM-type surface wave, resulting in the mentioned one-sided inductive loading.

This structure is thus a $5\lambda_0 \times 3\lambda_0$ metasurface with square patch unit cells over a dielectric substrate with a high permittivity $\epsilon_r = 10.2$, with thickness $d = 0.5$ mm, backed by a ground plane, as illustrated in Fig. 16. The unit-cell side is $l_u = 2.75$ mm and the patch side $l_p = 2.61$ mm. The

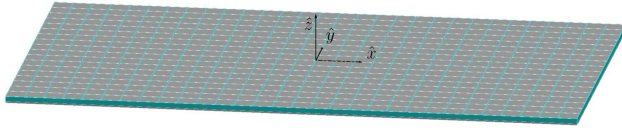


FIGURE 16. Reference Structure for the Ground Truth in Sec. V.B.1. The surface is illuminated from the top by an incident plane wave at 18 GHz.

structure is illuminated by a normally incident plane wave (i.e., coming from the top) and \hat{x} -polarized at 18 GHz. The equivalent IBC value corresponding to the unit-cell design of the original structure is $\mathcal{Z}_s = 834j$. The opaque impedance surface is discretized with mesh density $h \approx \lambda_0/13$ into triangular cells, such that the number of unknowns in the matrix problem is $N^\Lambda = 9817$.

2) Reference structure for transparent IBC test

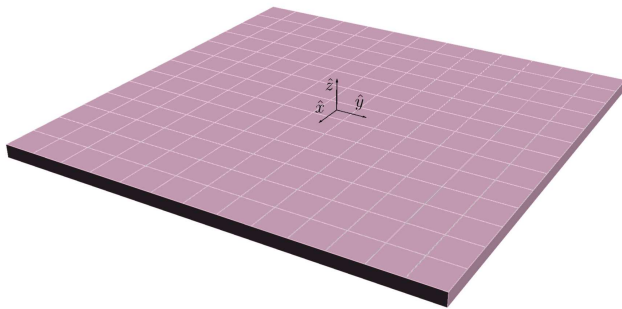


FIGURE 17. Reference Structure for the Ground Truth in Sec. V.B.2. The structure is $1\lambda_0 \times 1\lambda_0$ overall; the top surface is a wire grid, with wire width $l_s = 0.0154$ mm, atop a substrate of thickness $d = 0.5$ mm and relative permittivity $\epsilon_r = 3$. The structure is illuminated by a \hat{y} -polarized skew incident plane wave at 18 GHz, with $\theta^{\text{inc}} = 45^\circ$, $\phi^{\text{inc}} = 0^\circ$.

The reference structure for the transparent EFIE-IBC ground truth is done to achieve an inductive impedance sheet; this is obtained by a PEC wire grid, as shown in Fig. 17. This wire grid structure has a size of $1\lambda_0 \times 1\lambda_0$ and is positioned above a dielectric substrate with $\epsilon_r = 3$ and thickness $d = 0.5$ mm. A metallic ground plane is backing the substrate. The wires have a width $l_s = 0.0154$ mm, while each unit-cell has length side $l_u = 1.28$ mm; this corresponds to a sheet impedance of $\mathcal{Z}_s = 96.16j$. The plate is illuminated by a \hat{y} -polarized skew incident plane wave at 18 GHz, with $\theta^{\text{inc}} = 45^\circ$, $\phi^{\text{inc}} = 0^\circ$.

The EFIE-IBC includes the grounded dielectric slab, with the impedance sheet substituting the wire grid layer. The IBC is uniformly discretized with mesh density $h \approx \lambda_1/20$, resulting in a matrix problem with $N^\Lambda = 4272$ unknowns. A value of $\mathcal{Z}_s = 96.16j$ has been chosen, with reference to Fig. 4, as it yields an ill-posed problem.

C. CONSISTENCY

To demonstrate that the filtering technique does not worsen the results for well-posed EFIE-IBC formulations, we con-

sider the transparent study case presented in Section V.B.2. By setting a capacitive impedance value of $\mathcal{Z}_s = -600j$, we ensure the well-posedness of the transparent EFIE-IBC. This allows us to directly compare the scattered fields obtained from the standard and filtered EFIE-IBC formulations. As

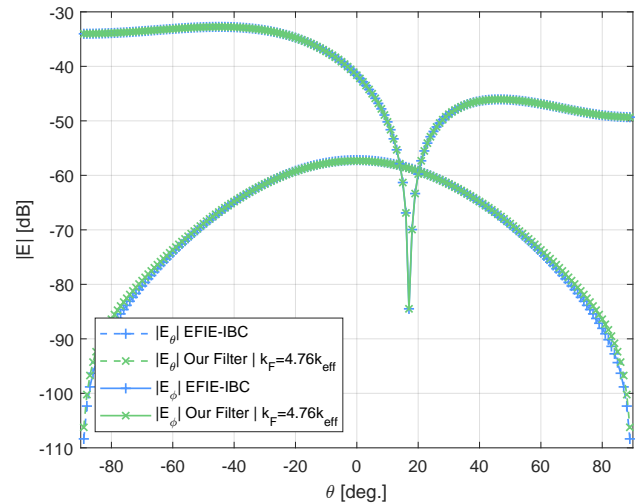


FIGURE 18. Scattered Electric Field (for cut $\phi = 0^\circ$) comparison between the original EFIE-IBC RWG and our filtered version for transparent capacitive scalar IBC value $\mathcal{Z}_s = -600j$. The normal incident plane illuminating the structure is \hat{x} -polarized.

shown in Figure 18, the two solutions exhibit excellent agreement, confirming the accuracy and reliability of our filtering approach for well-conditioned scenarios.

D. GROUND TRUTH TEST FOR OPAQUE REFERENCE STRUCTURE

As mentioned earlier on, the opaque IBC value considered here is set to $\mathcal{Z}_s^{\text{op}} = 834j$, corresponding to $\mathcal{Z}_s = \frac{1}{2}\mathcal{Z}_s^{\text{op}} = 417j$ as for Sec. II. This value strikes the “dangerous range” of the opaque EFIE-IBC producing eigenvalues zeroing; in our example, \mathcal{Z}_s is very close to one eigenvalue, $\zeta_c \approx -416.54j$.

To regularize this ill-posedness we employ the proposed wavenumber spectrum filtering, with wavenumber threshold k_F chosen to stay below the wavenumber spectrum associated with the critical eigenvalue (and so to avoid the Inaccessible Wavenumber Spectrum (IWS) area presented in Fig. 11).

Figure 19 shows that the proposed approach converges fast, due to the small condition number deriving from the preconditioning effect. The convergence of standard EFIE-IBC is not entirely problematic, despite the high condition number; we will comment further on this in the transparent case test, where it is more prominent. Indeed, the key part of the test is the comparison with the ground truth.

In this sense, Fig. 20 indicates that the proposed approach yields a faithful rendition of the ground truth. On the other hand, the discrepancy of the standard EFIE-IBC is an indication that the ill-posed problem here may end up

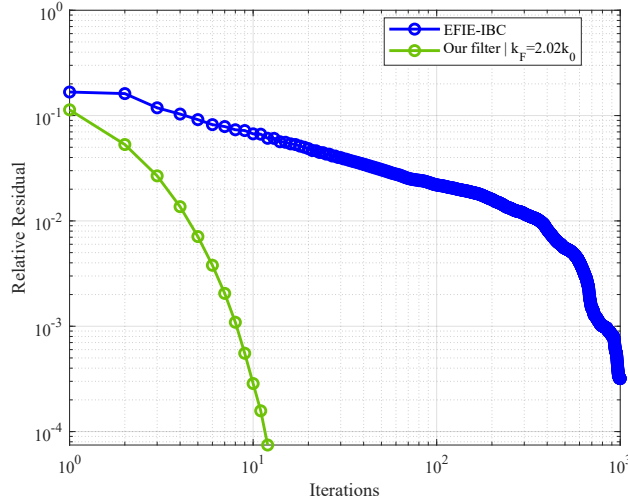


FIGURE 19. Reference Structure, Opaque case: Comparison of the convergence rates of the GMRES iterative solver for the two different formulations.

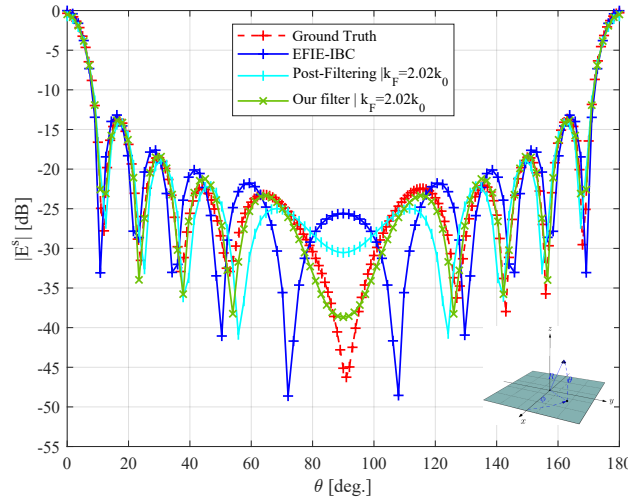


FIGURE 20. Ground truth comparison for the reference structure, opaque case with $\mathcal{Z}_s = 417j$, cut $\phi = 0^\circ$; normal incidence, polarization along \hat{x} . Ground truth, standard EFIE-IBC and spectral regularization; the curve “post filtering” refers to wavenumber filtering of the solution obtained with standard EFIE-IBC.

TABLE 1. Condition Number observed for Opaque Example

	RWG span	SBF Span ($k_F = 2.02k_0$)
PEC case	70.90	20.46
IBC $\mathcal{Z}_s = 417j$	1.96×10^4	9.02

in unexpected failure: it is evident that the non-regularized problem here ends in discrepancies that appear in the visible spectrum. This is a clear indication that the model equation, i.e., the EFIE-IBC equation, is not an entirely reliable model of the actual physical structure, i.e., the “ground truth” of the metasurface made of the unit cells in Fig. 16. This loss of fidelity to the ground truth can be attributed to the presence of near-zero eigenvalues of the EFIE-IBC, whose associated eigenfunctions have non-negligible components in the visible

(wavenumber) spectrum. This makes the regularization all the more important.

We observe that the regularized version shows a lower accuracy near grazing directions (angles beyond about 70°). This can be attributed to the fact that, in any case, the IBC is an approximation of real life.

Finally, we have also compared our method, which filters the wavenumber components in the employed basis, to an a-posteriori filtering of the wrong solution obtained by solving the standard EFIE-IBC. That is obtained by projecting the RWG solution onto the wavenumber-limited spectral basis used to obtain the regularized solution. Fig. 20 shows that this a-posteriori filtering reduces the error, but only partially.

E. GROUND TRUTH TEST FOR TRANSPARENT REFERENCE STRUCTURE

The employed sheet impedance value has been chosen in Sec. II to be near an eigenvalue, thus producing a near-zero eigenvalue of the EFIE-IBC; the regularization follows the discussion in Sec. IV.B, and from their graphical results (Fig. 9), the value of the cut-off wavenumber k_F is found. The results vis-à-vis the ground truth are collected in Fig. 22. As seen there, despite the minor effect of the (unmodulated) grating, the effect of near-zeroing an eigenvalue leads to a macroscopic error. Likewise, the regularization procedure restores values in accordance with the ground truth.

The GMRES convergence plots in Fig. 21 follow the same trend as for the opaque case, with the fast convergence of the regularized system. One can also see a non-intuitive result for the original, badly conditioned standard EFIE-IBC: while much slower, convergence to the set low residual threshold of 10^{-6} is attained without stagnation; this is all the more dangerous because it would lead to an undetected wrong result. It is observed that such a convergence strongly accelerates in a step-wise manner. This can be attributed to the presence of a few near-zero eigenvalues, that are eventually “captured” by the iterative solver.

We stress that, like in the previous opaque case, the choice of the problematic impedance values and cut-off wavenumber have been done using the approximate eigenvalues and their associated peak wavenumber deriving from the diagonal of the EFIE matrix in the spectral basis. This confirms the effectiveness of that approach in predicting problematic values of impedance, and effecting the regularization by filtering.

TABLE 2. Condition Number observed for the Transparent Example

	RWG span	SBF Span ($k_F = 1.96k_{\text{eff}}$)
PEC case	510.04	3.18
IBC $\mathcal{Z}_s = 96.16j$	1.13×10^6	1.33

VI. CONCLUSION

The Electric-Field Integral-Equation formulation of the IBC boundary-value problem (EFIE-IBC) has been shown to lead

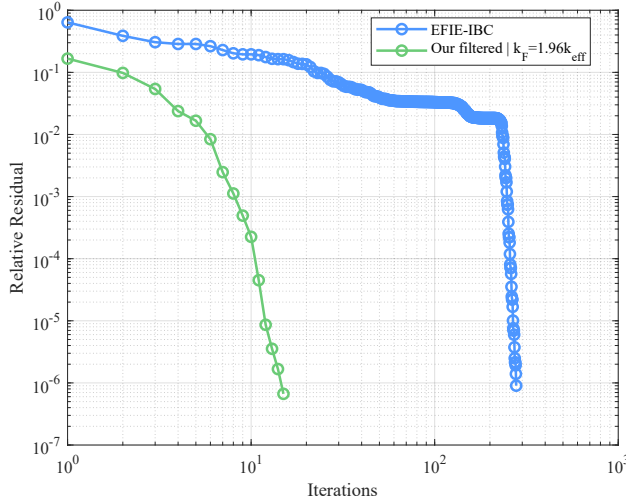


FIGURE 21. Reference Structure, Transparent case: Comparison of the convergence rates of the GMRES iterative solver for the two different formulations.

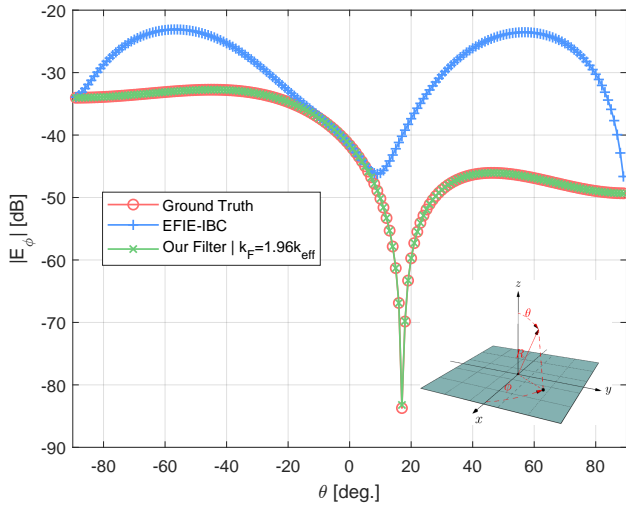


FIGURE 22. Ground truth comparison for the reference structure, transparent case, $Z_s = 96j$, cut $\phi = 0$; incidence along $\phi = 0$, $\theta^{inc} = 45^\circ$, polarization along \hat{x} . Ground truth, standard EFIE-IBC and spectral regularization.

to numerical instabilities for some impedance ranges of practical interest, in particular inductive reactances.

In this work, we have first analyzed the reason for the instability of the EFIE-IBC formulation, using the eigenvalues and eigenvectors of the EFIE and EFIE-IBC operators; this has shown that the reactive impedance loading can cause zeroing of eigenvalues; the important result is thus that the problem may become *ill-posed*, without a defined solution, and thus it is necessary to proceed to a *regularization* of the problem. The analysis suggests a regularization scheme based on the control of the wavenumber spectrum of the solution, which has been effected via a spectrally-resolved set of basis functions, in particular waveguide modes.

As the problem may be ill-posed, a specific evaluation methodology has been devised and implemented. We have

started from “physical” metasurface structures, which is what the IBC approximation purports to approximate; hence, the response of these structures constitutes the “ground truth” against which the solution of the IBC model has been compared. The solution of the unmodified EFIE-IBC appears wrong, and the symptoms of this malfunctioning appear difficult to detect. The solution of the regularized problem compares well with the ground truth.

This work has considered only scalar and spatially constant impedance. Ongoing work is in the direction to extend the method to modulated tensor impedance.

APPENDIX

A. RECTANGULAR WAVEGUIDE BASIS FUNCTIONS

The spectral basis functions here are the modes (eigenfunctions) of a Rectangular Waveguide with magnetic walls. We deal with an electric current $\mathbf{J} = \hat{\mathbf{n}} \times \mathbf{H}$, and will thus employ the magnetic eigenfunctions for the current; using the notation of Marcuvitz [36], $\mathbf{h}_{mn}^E, \mathbf{h}_{mn}^H$, $0 \leq m < M$, $0 \leq n < N$ [30], [36]. We further recall that in such a waveguide an $\hat{\mathbf{n}} \times$ operation maps electric eigenfunctions into magnetic ones, considering PMC wall vs. PEC walls, one finally gets

$$\Phi_i(\mathbf{r}) = \begin{cases} \mathbf{h}_{mn}^H(\mathbf{r}) & i = m(N-1) + n \\ \mathbf{h}_{mn}^E(\mathbf{r}) & i = MN - 1 + m(N-1) + n \end{cases} \quad (30)$$

where $\mathbf{h}^E, \mathbf{h}^H$ are the magnetic eigenfunctions of the rectangular waveguide (with side lengths a and b) with PEC walls:

$$\mathbf{h}_{mn}^H = \frac{2}{\sqrt{ab} k_{\rho mn}} \left(\frac{n\pi}{b} \sin\left(\frac{m\pi}{a}x\right) \cos\left(\frac{n\pi}{b}y\right) \hat{\mathbf{x}} - \frac{m\pi}{a} \cos\left(\frac{m\pi}{a}x\right) \sin\left(\frac{n\pi}{b}y\right) \hat{\mathbf{y}} \right) \quad (31)$$

$$\mathbf{h}_{mn}^E = \frac{\sqrt{\chi_m \chi_n}}{\sqrt{ab} k_{\rho mn}} \left(\frac{m\pi}{a} \sin\left(\frac{m\pi}{a}x\right) \cos\left(\frac{n\pi}{b}y\right) \hat{\mathbf{x}} + \frac{n\pi}{b} \cos\left(\frac{m\pi}{a}x\right) \sin\left(\frac{n\pi}{b}y\right) \hat{\mathbf{y}} \right) \quad (32)$$

where $\chi_m = 1$, if $m = 0$ and $\chi_m = 2, m \geq 1$. The total number of basis functions Φ obtained is $N^\Phi = 2MN - (M + N)$, where M and N are the highest mode indices in the $\hat{\mathbf{x}}$ and $\hat{\mathbf{y}}$ directions.

B. REACTANCE OF SQUARE PATCH AND SQUARE WIRE GRID UNIT-CELLS

This appendix collects the approximate analytical results of [33] in graphical form; the graphs also indicate the reactance regions resulting in ill-conditioned EFIE-IBC and possibly ill-posedness. The results imply the periodic approximation (as usual). If the dielectric does not play a role in the wire grid transparent IBC value, it remains a relevant parameter in its complementary structure.

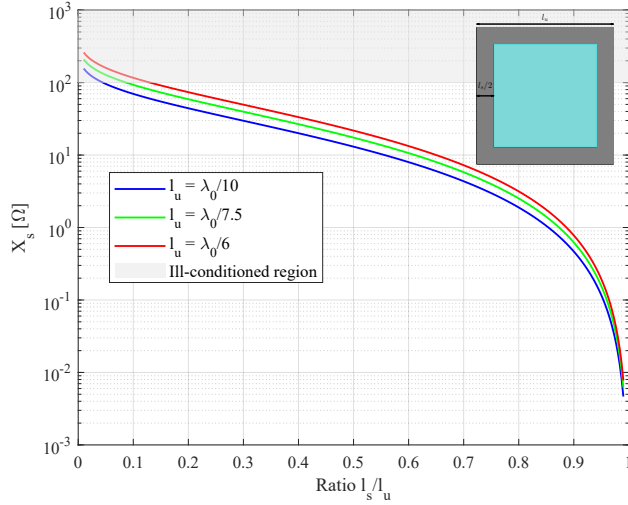


FIGURE 23. Reactance of a square wire grid unit-cell of length side l_u illuminated by a normal incident plane wave. The wire width is defined as l_s . The graph is relevant to transparent IBC.

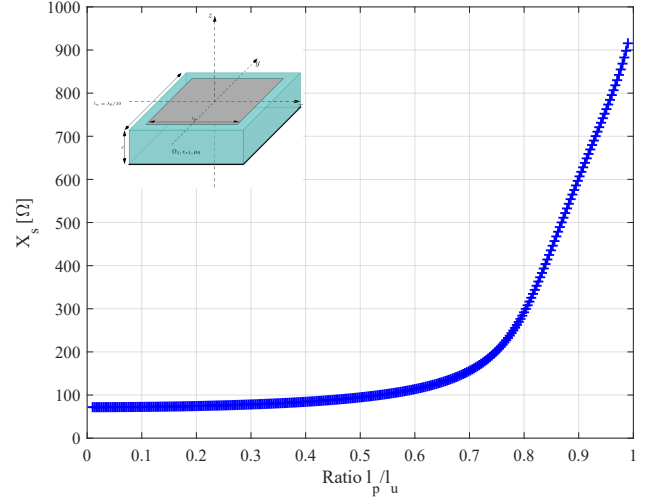


FIGURE 25. Opaque IBC scalar values $Z_s^{\text{op}} = jX_s$ of a square patch unit-cell of length side l_u illuminated by a normal incident plane wave, and backed by a dielectric substrate $\epsilon_r = 10.2$ and a ground plane. The graph is relevant to the opaque IBC example.

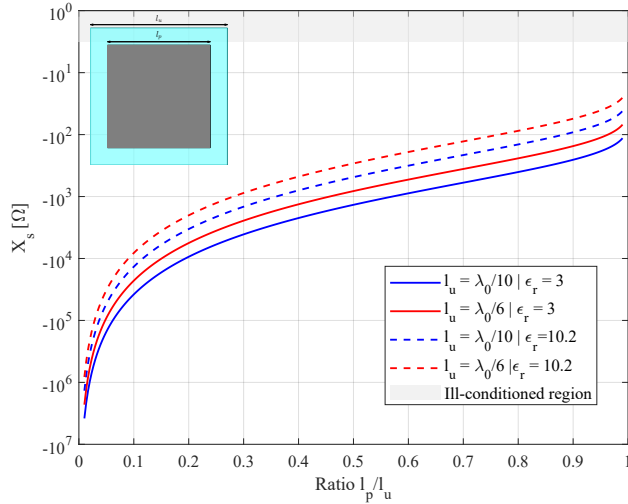


FIGURE 24. Reactance of a square patch unit-cell of length side l_u illuminated by a normal incident plane wave. The graph is relevant to the transparent IBC value of the patch surface.

The opaque IBC values presented in Fig. 25 are obtained [11], under the solution of the Transverse Resonance Equation (TRE) for normal incidence,

$$(Z_s^{\text{op}})^{-1} = (Z_s^t)^{-1} - j\sqrt{\frac{\epsilon_1}{\mu_1}} \cot(k_{z1}d) \quad (33)$$

to take in account the effect of the dielectric slab into the IBC value.

References

[1] C. L. Holloway, E. F. Kuester, J. A. Gordon, J. O'Hara, J. Booth, and D. R. Smith, "An overview of the theory and applications of metasurfaces: The two-dimensional equivalents of metamaterials," *IEEE Antennas and Propagation Magazine*,

[2] Y. Liu, X. Liu, X. Mu, *et al.*, "Reconfigurable Intelligent Surfaces: Principles and Opportunities," *IEEE Communications Surveys & Tutorials*, vol. 23, no. 3, pp. 1546–1577, 2021. DOI: 10.1109/COMST.2021.3077737.

[3] Q. Wu, B. Zheng, C. You, *et al.*, "Intelligent Surfaces Empowered Wireless Network: Recent Advances and the Road to 6G," *Proceedings of the IEEE*, vol. 112, no. 7, pp. 724–763, 2024. DOI: 10.1109/JPROC.2024.3397910.

[4] G. Oliveri, P. Rocca, M. Salucci, and A. Massa, "Holographic Smart EM Skins for Advanced Beam Power Shaping in Next Generation Wireless Environments," *IEEE Journal on Multiscale and Multiphysics Computational Techniques*, vol. 6, pp. 171–182, 2021. DOI: 10.1109/JMMCT.2021.3121300.

[5] T. B. A. Senior and J. L. Volakis, *Approximate Boundary conditions in electromagnetism* (IEEE Electromagnetic Waves Series). The Institution of Electrical Engineers, 1995, vol. 41, ISBN: 978-0-85296-849-9.

[6] A. Karlsson, "Approximate Boundary Conditions for Thin Structures," *IEEE Transactions on Antennas and Propagation*, vol. 57, no. 1, pp. 144–148, 2009. DOI: 10.1109/TAP.2008.2009720.

[7] P. J. B. Clarricoats and A. D. Olver, *Corrugated Horns for Microwave Antennas (IEEE Electromagnetic Waves)*. The Institution of Engineering and Technology, 1984. DOI: 10.1049/PBEW018E.

[8] M. Beruete, I. Campillo, J. Dolado, *et al.*, "Very low-profile "Bull's Eye" feeder antenna," *IEEE Antennas and Wireless Propagation Letters*, vol. 4, pp. 365–368, 2005. DOI: 10.1109/LAWP.2005.851104.

[9] E. Martini and S. Maci, "Metasurface Transformation Theory," in *Transformation Electromagnetics and Metamaterials: Fundamental Principles and Applications*, D. H. Werner and D.-H. Kwon, Eds. London: Springer London, 2014, pp. 83–116. DOI: 10.1007/978-1-4471-4996-5_3.

[10] M. Faenzi, G. Minatti, D. González-Ovejero, *et al.*, "Metasurface Antennas: New Models, Applications and Realizations," *Scientific*

- Reports*, vol. 9, no. 1, p. 10 178, 2019, ISSN: 2045-2322. DOI: 10.1038/s41598-019-46522-z.
- [11] M. A. Francavilla, E. Martini, S. Maci, and G. Vecchi, "On the Numerical Simulation of Metasurfaces With Impedance Boundary Condition Integral Equations," *IEEE Transactions on Antennas and Propagation*, vol. 63, no. 5, pp. 2153–2161, 2015. DOI: 10.1109/TAP.2015.2407372.
- [12] S. Yan and J.-M. Jin, "Self-Dual Integral Equations for Electromagnetic Scattering From IBC Objects," *IEEE Transactions on Antennas and Propagation*, vol. 61, no. 11, pp. 5533–5546, 2013. DOI: 10.1109/TAP.2013.2276929.
- [13] A. J. Poggio and E. K. Miller, "Integral Equation Solutions of Three-dimensional Scattering Problems," in *Computer Techniques for Electromagnetics*, ser. International Series of Monographs in Electrical Engineering, R. Mittra, Ed., Pergamon, 1973, pp. 159–264, ISBN: 978-0-08-016888-3. DOI: <https://doi.org/10.1016/B978-0-08-016888-3.50008-8>.
- [14] M. Movahediqomi, G. Ptitcyn, and S. Tretyakov, *Comparison Between Different Designs and Realizations of Anomalous Reflectors*, 2023. eprint: 2301.02851.
- [15] D. González-Ovejero, C. Jung-Kubiak, M. Alonso-delPino, T. Reck, and G. Chattopadhyay, "Design, fabrication and testing of a modulated metasurface antenna at 300 GHz," in *2017 11th European Conference on Antennas and Propagation (EUCAP)*, 2017, pp. 3416–3418. DOI: 10.23919/EuCAP.2017.7928611.
- [16] D. Sievenpiper, L. Zhang, R. Broas, N. Alexopolous, and E. Yablonovitch, "High-impedance electromagnetic surfaces with a forbidden frequency band," *IEEE Transactions on Microwave Theory and Techniques*, vol. 47, no. 11, pp. 2059–2074, 1999. DOI: 10.1109/22.798001.
- [17] B. H. Fong, J. S. Colburn, J. J. Ottusch, J. L. Visher, and D. F. Sievenpiper, "Scalar and Tensor Holographic Artificial Impedance Surfaces," *IEEE Transactions on Antennas and Propagation*, vol. 58, no. 10, pp. 3212–3221, 2010. DOI: 10.1109/TAP.2010.2055812.
- [18] M. Bruliard and G. Vecchi, "Stabilization of EFIE-IBC by Spatial Filtering," in *2024 — 18th European Conference on Antennas and Propagation (EUCAP)*, 2024, pp. 3299–3301, ISBN: 978-88-31299-09-1.
- [19] K. Michalski and J. Mosig, "Multilayered media Green's functions in integral equation formulations," *IEEE Transactions on Antennas and Propagation*, vol. 45, no. 3, pp. 508–519, Mar. 1997. DOI: 10.1109/8.558666.
- [20] S. Rao, D. Wilton, and A. Glisson, "Electromagnetic scattering by surfaces of arbitrary shape," *IEEE Transactions on Antennas and Propagation*, vol. 30, no. 3, pp. 409–418, 1982. DOI: 10.1109/TAP.1982.1142818.
- [21] I. Fredholm, "Sur une classe d'équations fonctionnelles," *Acta Mathematica*, vol. 27, pp. 365–390, 1903.
- [22] W. Chew, E. Michielssen, J. M. Song, and J. M. Jin, *Fast and Efficient Algorithms in Computational Electromagnetics*. Artech House, Inc., 2001, ISBN: 1580531520.
- [23] J. M. Jin, *Basic Electromagnetic Theory*. John Wiley & Sons, Ltd, 2010, ISBN: 9780470874257.
- [24] S. B. Adrian, A. Dély, D. Consoli, A. Merlini, and F. P. Andriulli, "Electromagnetic Integral Equations: Insights in Conditioning and Preconditioning," *IEEE Open Journal of Antennas and Propagation*, vol. 2, pp. 1143–1174, 2021. DOI: 10.1109/OJAP.2021.3121097.
- [25] G. Vecchi, "Loop-Star decomposition of basis functions in the discretization of the EFIE," *IEEE Trans. Antennas Propag.*, vol. 47, no. 2, pp. 339–346, Feb. 1999.
- [26] R.-C. Li, "Matrix Perturbation Theory," in *Handbook of Linear Algebra*, Chapman and Hall/CRC, 2013, pp. 15–1 –15–17, ISBN: 1-58488-510-6.
- [27] F. Vipiana, P. Pirinoli, and G. Vecchi, "Spectral Properties of the EFIE-MoM Matrix for Dense Meshes With Different Types of Bases," *IEEE Transactions on Antennas and Propagation*, vol. 55, pp. 3229–3238, Nov. 2007, ISSN: 1558-2221. DOI: 10.1109/TAP.2007.908827.
- [28] G. Vecchi, P. Pirinoli, and M. Orefice, "On the use of cavity modes as basis functions in the full wave analysis of printed antennas," *IEEE Transactions on Antennas and Propagation*, vol. 46, no. 4, pp. 589–594, 1998. DOI: 10.1109/8.664125.
- [29] M. Casaletti, S. Maci, and G. Vecchi, "A complete set of linear-phase basis functions for scatterers with flat faces and for planar apertures," *IEEE Transactions on Antennas and Propagation*, vol. 59, no. 2, pp. 563–573, 2011. DOI: 10.1109/TAP.2010.2096178.
- [30] F. Verni, M. Righero, and G. Vecchi, "On the Use of Entire-Domain Basis Functions and Fast Factorizations for the Design of Modulated Metasurface," *IEEE Transactions on Antennas and Propagation*, vol. 68, no. 5, pp. 3824–3833, 2020. DOI: 10.1109/TAP.2020.2966040.
- [31] A. Freni, P. De Vita, P. Pirinoli, L. Matekovits, and G. Vecchi, "Fast-factorization acceleration of mom compressive domain-decomposition," *IEEE Transactions on Antennas and Propagation*, vol. 59, no. 12, pp. 4588–4599, 2011. DOI: 10.1109/TAP.2011.2165474.
- [32] W. H. Press, S. A. Teukolsky, W. T. Vetterling, and B. P. Flannery, *Numerical Recipes 3rd Edition: The Art of Scientific Computing*, 3rd ed. USA: Cambridge University Press, 2007, ISBN: 0521880688.
- [33] O. Luukkonen, C. Simovski, G. Granet, et al., "Simple and Accurate Analytical Model of Planar Grids and High-Impedance Surfaces Comprising Metal Strips or Patches," *IEEE Transactions on Antennas and Propagation*, vol. 56, no. 6, pp. 1624–1632, 2008. DOI: 10.1109/TAP.2008.923327.
- [34] Dassault Systèmes Simulia, *CST Studio Suite®*. [Online]. Available: www.cst.com.
- [35] A. M. Patel and A. Grbic, "Modeling and Analysis of Printed-Circuit Tensor Impedance Surfaces," *IEEE Transactions on Antennas and Propagation*, vol. 61, no. 1, pp. 211–220, 2013. DOI: 10.1109/TAP.2012.2220092.
- [36] N. Marcuvitz, "Transmission-line modes," in *Waveguide Handbook (IEEE Electromagnetic Waves Series)*. McGraw-Hill, 1951, vol. 21, ch. 2, pp. 55–100.



Margaux Bruliard (Graduate Student Member, IEEE) received the B.Sc. degrees in Applied Mathematics and Computer Science in 2017, and subsequently, her M.Sc. Eng degree in Scientific Computing Methods and Applied Mathematics from the Université Sorbonne Paris Nord (France) in 2019.

She is currently a Ph.D. student at Politecnico di Torino, Turin, Italy, and focuses her research work on developing improved mathematical models for impedance boundary conditions and meta-surfaces in electromagnetic simulations.



Marcello Zucchi (Member, IEEE) received the B.Sc. degree in electronics and telecommunications engineering from the University of Bologna, Bologna, Italy, in 2014, the M.Sc. degree in electronics engineering and the Ph.D. in electrical, electronics and communications engineering from Politecnico di Torino, Turin, Italy, in 2018 and 2022, respectively.

In 2023, he joined the Department of Electronics and Telecommunications, Politecnico di Torino, as a postdoctoral researcher. His research interests

include global optimization algorithms for flat antenna design, automatic synthesis of metasurface antennas and field focusing algorithms for hyperthermia treatment.



Giuseppe Vecchi (Life Fellow, IEEE) received the Laurea and Ph.D. degrees in electronic engineering from the Politecnico di Torino, Turin, Italy, in 1985 and 1989, respectively, with doctoral research carried out partly at Polytechnic University, Farmingdale, NY, USA.

He was a Visiting Scientist with Polytechnic University of NY from 1989 to 1990. Since 1990, he has been with the Department of Electronics, Politecnico di Torino, as an Assistant Professor, an Associate Professor from 1992 to 2000, and a Professor since 2000. He was a Visiting Scientist with the University of Helsinki, Helsinki, Finland, in 1992, and has been an Adjunct Faculty with the Department of Electrical and Computer Engineering, University of Illinois at Chicago, Chicago, IL, USA, from 1997 to 2011. Since 2015, he has been serving as the Director of the Antenna and EMC Laboratory (LACE), Politecnico di Torino.

His current research activities concern analytical and numerical techniques for design, measurement, and diagnostics of antennas and devices, medical applications, and imaging.

Prof. Vecchi is a member of the Board of the European School of Antennas (ESOA) and the IEEE Antennas and Propagation Standard Committee. He has been an Associate Editor of the IEEE TRANSACTIONS ON ANTENNAS AND PROPAGATION, the Chairman of the IEEE AP/MTT/ED Italian joint Chapter, and a member of the IEEE-APS Educational Committee.